

Steady-state and equilibrium vortex configurations, transitions, and evolution in a mesoscopic superconducting cylinder

Sangbum Kim

Department of Mechanical engineering, Texas A&M University, College Station, Texas 77843

Chia-Ren Hu

Center for Theoretical Physics, Department of Physics, Texas A&M University, College Station, Texas 77843

Malcolm J. Andrews

Department of Mechanical engineering, Texas A&M University, College Station, Texas 77843

(January 13, 2003)

A numerical scheme to study the mixed states in a mesoscopic type-II superconducting cylinder is described. Steady-state configurations and transient behavior of the magnetic vortices for various values of the applied magnetic field H are presented. Transitions between different multi-vortex states as H is changed is demonstrated by contour plots and jumps in the B vs H plot. Evolving a uniformly-superconducting initial state using the simplest set of relaxation equations shows that the system passes through nearly metastable intermediate configurations, while seeking the final minimum-energy, steady state consistent with the square symmetry of the sample. An efficient scheme to determine the equilibrium vortex configuration in a mesoscopic system at any given applied field, not limited to the symmetry of the system, is devised and demonstrated.

PACS numbers: 79.60.Bm, 73.20.Dx, 74.72.-h

I. INTRODUCTION

The electromagnetic characteristics of type-II superconductors have been of great interest, particularly since the discovery of high-temperature superconductors. Furthermore, a recent surge in interest about nano-technology, has drawn the attention of researchers from various disciplines to a detailed understanding of the characteristics of mesoscopic superconducting samples. Several phenomenological theories have been developed during decades of superconductor research, one popular choice is the Ginzburg-Landau theory.^{1,2} Its time-dependent extension is known as Time-Dependent Ginzburg-Landau (TDGL) theory.³

In the Ginzburg-Landau theory, the electromagnetic state of a superconductor can be determined by solving a system of partial differential equations. It was discovered by Abrikosov that if the κ parameter that appears in the equations, now known as the Ginzburg-Landau parameter, is larger than $1/\sqrt{2}$, then when a bulk superconductor is placed in a sufficiently large magnetic field, the magnetic field penetrates the superconductor in the form of singly-quantized vortices. Around each vortex flows a supercurrent,⁴ confining a single quantum of magnetic flux within it. Superconductors with this property are known as type-II.

Here we present the result of a numerical study about the magnetization process inside a superconducting cylinder with sub-micron lateral dimension in an external magnetic field. We have restricted the work to a square cross section of a linear size equal to 4.65 times λ (the magnetic penetration depth). A typical value for λ

is about 500 Å, and then the cross-sectional area is about $0.054 \mu\text{m}^2$.

Previous works on the magnetization of a mesoscopic superconductor without pinning centers have been reported by Peeters *et al.*⁵⁻⁸ and others^{9,10}, who have presented extensive calculations on the superconducting state in mesoscopic, type-I, superconducting thin films. In most cases they found transitions between giant vortex states of different circulation quantum numbers L , with some multi-vortex states occasionally appearing as thermodynamically stable states, but mostly as metastable states. These predictions appear to have already received some level of experimental confirmation, although some discrepancies still exist¹¹. (Ref.¹⁰ have mainly compared the energy of a "3-2" vortex-antivortex molecule state with that of a single off-centered vortex state at $L = 1$, as both evolve to the equilibrium state of a single vortex at the center.) Misko *et al.*¹² have studied both type-I and type-II mesoscopic triangular cylinders, and have shown that a vortex-antivortex molecule appears only if the sample is type-I. They considered only one field value at which $L = 2$ is favored, and did not consider vortex configurational transitions as the field changes.¹³

Our aim is to simulate how vortices enter and settle in stable arrangements when a mesoscopic type-II superconductor of a given symmetry is first cooled below the critical temperature, and then an external magnetic field is applied. This is often termed zero field cooling (ZFC). We find that only vortex numbers and configurations consistent with the sample symmetry can appear in this case. It is known that there exist global minimum-energy vortex configurations with reduced symmetry, correspond-

ingly to final equilibrium states at general values of the applied field. To find these equilibrium states we developed, and demonstrate here, an efficient numerical scheme.

Our approach is to solve a set of simplified (and discretized) TDGL equations, in which the coupling to the electric field is neglected, and the superconducting order parameter and the magnetic field are assumed to relax with the same time scale. These assumptions are not physical, but are acceptable here, since we are only interested in obtaining the final steady-state vortex configurations, and the symmetry-related qualitative behavior of the transient configurations and their evolution. (For a more physical set of TDGL equations see Tinkham³. For an example of numerical solution of such a set of TDGL equations, see¹⁴.) However, since the equations we have solved do not contain any thermal fluctuation terms, and the sample we considered has a perfect square symmetry, we find that when starting with the Meissner state with no field penetration, then the final steady-state vortex configurations we obtain all have perfect square symmetry, with vortex numbers also limited to only multiples of four (the symmetry number). These configurations would correspond to physical situations under zero-field cooling, if the physical sample has indeed perfect symmetry, and the temperature is sufficiently low, so that thermal fluctuations are not able to overcome any energy barrier for vortex entry, expulsion, or rearrangement. However, if the sample surface has slight imperfection, or if the temperature is not sufficiently low, then these configurations are, in most cases, not in equilibrium at the given magnetic field strength. Even the vortex number may not be correct. However, if we insert into the equations terms to simulate thermal fluctuation, as in the method of simulated annealing,^{15,17} then the simulation program will take a much longer time to run, and may become impractical even with a supercomputer. So we have devised an efficient scheme to find the equilibrium vortex configurations: We solve the same set of relaxation equations without any thermal fluctuation terms. But instead of starting the solution with the Meissner state as the initial state, we devise artificial initial states with a given number of vortices in random positions. We present analytic expressions for such initial states, in terms of a widely known approximate expression for a singly-quantized vortex in cylinder coordinates. Then for vortex numbers not too different from the equilibrium number, the final steady states obtained by solving our relaxation equations will, in most cases, have the number of vortices close to those of the initial states. By comparing the total Gibbs energies of these steady states with different vortex numbers — sometimes we obtain more than one configuration for the same vortex number, (when the vortex number exceeds four,) then their Gibbs energies are also compared — we can find the state with the lowest total Gibbs energy, which we identify as the equilibrium state with the equilibrium vortex number. We give an explicit demonstration of this scheme¹⁸,

that might be very useful in view of the recent interest in nanoscience and nanotechnology. In some nano-applications one may need to find the equilibrium vortex configurations in a mesoscopic superconducting sample, at different applied magnetic fields. We note that in a bulk sample vortices like to form a triangular lattice. Thus, when the sample does not conform with this symmetry, and if the sample is sufficiently small so that the boundary effect on the equilibrium vortex configurations is important, then the system is frustrated, and the equilibrium vortex configurations can be quite intriguing, and difficult to foresee. The scheme devised here is then very convenient and useful for finding the answer.¹⁶

II. TIME-DEPENDENT GINZBURG-LANDAU MODEL

In an external magnetic field \mathbf{H} , the Gibbs free energy density g of a superconducting state is given by³

$$g = f_n + \alpha|\Psi|^2 + \frac{\beta}{2}|\Psi|^4 + \frac{1}{2m_s} \left| \left(-i\hbar\nabla - \frac{e_s}{c}\mathbf{A} \right) \Psi \right|^2 + \frac{|\mathbf{h}|^2}{8\pi} - \frac{\mathbf{h} \cdot \mathbf{H}}{4\pi} \quad (1)$$

where f_n is the free energy density in the normal state in the absence of the field, Ψ is the complex-valued order parameter, with the superscript * denoting complex conjugation, \mathbf{A} the magnetic vector potential, $\mathbf{h} = \nabla \times \mathbf{A}$ the induced magnetic field and \mathbf{H} the applied magnetic field. The supercurrent density is expressed as $\mathbf{J}_s = \nabla \times \nabla \times \mathbf{A} = \frac{e_s\hbar}{2im_s} (\Psi^*\nabla\Psi - \Psi\nabla\Psi^*) - \frac{e_s^2}{m_sc} |\Psi|^2 \mathbf{A}$. In the above e_s is the "effective charge" of a Cooper pair which is twice the charge of an electron, and m_s its "effective mass" which can be selected arbitrarily, but the conventional choice is twice the mass of an electron. Also, c is the speed of light, and $\hbar = h/2\pi$ where h is Planck's constant.

Ginzburg-Landau theory postulates that the Gibbs free energy of a superconducting sample Ω , $G(\Psi, \mathbf{A}) = \int_{\Omega} g d\Omega$ is at a minimum in the superconducting state. The celebrated Ginzburg-Landau equations are obtained by minimizing this functional with respect to Ψ and \mathbf{A} using the variational principle.

Since a constant term does not change the end result of the variational technique, an algebraic manipulation is made to subtract f_n and add $\mathbf{H} \cdot \mathbf{H}/8\pi$ to the g above, giving¹⁹

$$G(\Psi, \mathbf{A}) = \int_{\Omega} \left(\alpha|\Psi|^2 + \frac{\beta}{2}|\Psi|^4 + \frac{|\mathbf{h} - \mathbf{H}|^2}{8\pi} + \frac{1}{2m_s} \left| \left(-i\hbar\nabla - \frac{e_s}{c}\mathbf{A} \right) \Psi \right|^2 \right) d\Omega \quad (2)$$

Nondimensionalizing variables as

$$x' = \frac{x}{\lambda}, \mathbf{H}' = \frac{\mathbf{H}}{\sqrt{2}H_c}, \mathbf{h}' = \frac{\mathbf{h}}{\sqrt{2}H_c}, \mathbf{j}' = \frac{2\sqrt{2}\pi\lambda}{cH_c} \mathbf{j}, \mathbf{A}' = \frac{\mathbf{A}}{\sqrt{2}H_c\lambda}, \Psi' = \frac{\Psi}{\Psi_0}. \text{ The characteristic scales are:}$$

$|\Psi_0| = \sqrt{-\alpha/\beta}$ which is the magnitude of Ψ that minimizes the free energy in the absence of a field; the thermodynamic critical field strength $H_c = \left(4\pi|\alpha||\Psi_0|^2\right)^{1/2}$, which divides the normal state and superconducting state regions in Type-I superconductor phase diagram; the London penetration depth $\lambda = \left(\frac{m_s c^2}{4\pi|\Psi_0|^2 e_s^2}\right)^{1/2}$; the coherence length $\xi = \left(\frac{\hbar^2}{2m_s|\alpha|}\right)^{1/2}$; and, the Ginzburg-Landau parameter $\kappa = \lambda/\xi$.

We obtain the dimensionless gauge-invariant free energy functional (omitting primes for convenience),

$$G(\Psi, \mathbf{A}) = \int_{\Omega} \left(-|\Psi|^2 + \frac{1}{2}|\Psi|^4 + |\nabla \times \mathbf{A} - \mathbf{H}|^2 + \left| \left(\frac{\nabla}{\kappa} - i\mathbf{A} \right) \Psi \right|^2 \right) d\Omega \quad (3)$$

The simplified TDGL model we employ to find solutions of the static GL equations may be viewed as a gradient flow with the energy functional. That is, the variation of (Ψ, \mathbf{A}) w.r.t. time should be in the opposite direction of the gradient of the energy functional, $\frac{\partial \Psi}{\partial t} = -\frac{\partial G}{\partial \Psi^*}$, $\frac{\partial \mathbf{A}}{\partial t} = -\frac{1}{2} \frac{\partial G}{\partial \mathbf{A}}$ with time, t , in units of the only relaxation time of the equations. The natural boundary conditions are: (1) the continuity of the parallel component of the magnetic field across the boundary surface: $(\nabla \times \mathbf{A}) \times \mathbf{n} = \mathbf{H} \times \mathbf{n}$, (for two-dimensional problems only, see below) and (2) the vanishing gauge-invariant normal derivative of Ψ : $\left(\frac{\nabla}{\kappa} - i\mathbf{A}\right) \Psi \cdot \mathbf{n} = 0$,²⁰ with \mathbf{n} denoting the outward surface normal.

III. DISCRETIZATION AND CALCULATION PROCEDURE

For long cylindrical samples, we need only solve a 2-D problem. We take $\mathbf{A} = (A(x, y), B(x, y), 0)$ and $\mathbf{H} = (0, 0, H)$ where $H = (\nabla \times \mathbf{A})_z = \frac{\partial B}{\partial x} - \frac{\partial A}{\partial y}$.

Defining the link variables as below, the gauge invariance is preserved in discretizing the Gibbs free energy and the consequent TDGL equations. $W(x, y) = \exp(i\kappa \int^x A(\zeta, y) d\zeta)$, $V(x, y) = \exp(i\kappa \int^y B(x, \eta) d\eta)$. Noting that $|\partial_x(W^*\Psi)| = |(\partial_x - i\kappa A)\Psi|$, and $|\partial_y(V^*\Psi)| = |(\partial_y - i\kappa B)\Psi|$, we have

$$G(\Psi, \mathbf{A}) = \int_{\Omega} \left(-|\Psi|^2 + \frac{1}{2}|\Psi|^4 + |\nabla \times \mathbf{A} - \mathbf{H}|^2 + \left| \frac{1}{\kappa} \partial_x(W^*\Psi) \right|^2 + \left| \frac{1}{\kappa} \partial_y(V^*\Psi) \right|^2 \right) d\Omega. \quad (4)$$

We discretize the free energy functional on a staggered grid in Ω shown in Fig. 1.^{21,22} This gives us a second-order approximation in h_x and h_y to the continuous energy functional, where the h_x and h_y are the spatial increments in the x- and y-direction. The staggered grid

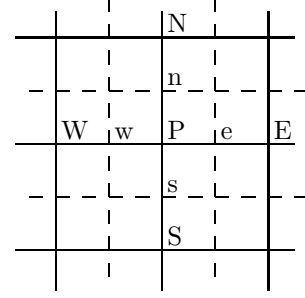


FIG. 1. Staggered Grid

also leads to a satisfactory way of discretizing the natural boundary conditions.²³ For a rectangular grid, the first component of the vector potential is constant in time on one pair of the edges of the boundary, and the second component is constant in time on the other pair.²⁰

In this paper, we assume that the cylindrical superconductor has a square cross-section and is subject to an applied field along the cylindrical axis. The applied field is assumed to be constant in time. We further assume the order parameter Ψ varies in the cross-sectional plane of the cylindrical sample, and the vector potential \mathbf{A} has only two nonzero components (A, B) , which also lie in this plane. We also assume that the superconductor has no pinning sites. Then at steady-state conditions, the vortices settle in maximal distances due to the repulsion of each other. This requirement leads to triangular lattice of vortices in an infinitely large domain.³

In the staggered grid the lattice points for Ψ , A , and B are all different, with Ψ evaluated at the node center (i, j) , A evaluated at the east cell face $(i+1/2, j)$, and B evaluated at the north cell face $(i, j+1/2)$. According to Refs. 21, 22, this formulation keeps second order accuracy in the derivative evaluations as they appear in each of the discretized equations.

Now the discrete TDGL is obtained by minimizing the discrete energy functional G_d with respect to the variation in Ψ and \mathbf{A} as

$$\frac{\partial \Psi_P}{\partial t} = \frac{h_x h_y}{\kappa^2} \left(\frac{e^{iA_w \kappa h_x} \Psi_W - 2\Psi_P + e^{-iA_e \kappa h_x} \Psi_E + e^{iB_s \kappa h_y} \Psi_S - 2\Psi_P + e^{-iB_n \kappa h_y} \Psi_N}{h_x^2 h_y^2} \right) + h_x h_y N_1(\Psi_P) \quad (5)$$

$$\frac{\partial A_e}{\partial t} = -h_x \left(\frac{B_n E - B_n + B_s - B_s E - A_{Ne} - 2A_e + A_{Se}}{h_x h_y} \right) + \frac{h_y}{\kappa} N_2(A_e, \Psi_P, \Psi_E) \quad (6)$$

$$\frac{\partial B_n}{\partial t} = -h_y \left(\frac{A_w - A_e + A_{Ne} - A_{Nw}}{h_y} \right)$$

$$\frac{B_{nE} - 2B_n + B_{nW}}{h_x} \Big) + \frac{h_x}{\kappa} N_3(B_n, \Psi_P, \Psi_N) \quad (7)$$

where

$$N_1(\Psi_P) = (1 - |\Psi_P|^2) \Psi_P \quad (8)$$

$$N_2(A_e, \Psi_P, \Psi_E) = (\Phi_P \Theta_E - \Theta_P \Phi_E) \cos(A_e \kappa h_x) - (\Phi_P \Phi_E + \Theta_P \Theta_E) \sin(A_e \kappa h_x)$$

$$N_3(B_n, \Psi_P, \Psi_N) = (\Phi_P \Theta_N - \Theta_P \Phi_N) \cos(B_n \kappa h_y) - (\Phi_P \Phi_N + \Theta_P \Theta_N) \sin(B_n \kappa h_y)$$

where Θ and Φ are the real and imaginary parts of Ψ , and boundary conditions of the computational domain Ω (with T , B , L , and R denoting top, bottom, left, and right, respectively):

$$\Psi_P = \Psi_S e^{\nu \kappa h_y B_s}, \text{ on } \Omega_T \quad (9)$$

$$\Psi_P = \Psi_N e^{-\nu \kappa h_y B_n}, \text{ on } \Omega_B \quad (10)$$

$$\Psi_P = \Psi_E e^{-\nu \kappa h_x A_e}, \text{ on } \Omega_L \quad (11)$$

$$\Psi_P = \Psi_W e^{\nu \kappa h_x A_w}, \text{ on } \Omega_R \quad (12)$$

$$A_e = A_{Se} - \left(H - \frac{B_{nE} - B_n}{h_x} \right) h_y \text{ on } \Omega_T \quad (13)$$

$$A_e = A_{Ne} + \left(H - \frac{B_{nE} - B_n}{h_x} \right) h_y \text{ on } \Omega_B \quad (14)$$

$$B_n = B_{nE} - \left(H + \frac{A_{Ne} - A_e}{h_y} \right) h_x \text{ on } \Omega_L \quad (15)$$

$$B_n = B_{nW} + \left(H + \frac{A_{Ne} - A_e}{h_y} \right) h_x \text{ on } \Omega_R \quad (16)$$

The finite difference equations are solved by the Euler method with $h_x = h_y = 0.15$ and $\Delta t = 0.05$, and taking $\kappa = 4$. In the numerical computations that follow, everything is kept the same except for the strength of the applied magnetic field and/or the initial conditions.

IV. STEADY STATES UNDER ZERO-FIELD COOLING IN A PERFECTLY SQUARE SAMPLE AT LOW TEMPERATURES

We first solve the above set of equations assuming that the initial state is the perfect Meissner state with no field penetration. As explained in the introduction, this corresponds to applying a magnetic field after zero-field cooling. Fig. 2 shows the plots of $|\Psi|^2$ [the left figure in (a) through (k)] and $h = \nabla \times \mathbf{A}$ [the right figure in (a) through (k)] for the final steady states reached at a sequence of increasing H values. In the left figures $|\Psi|^2$, which is interpreted physically as the density of Cooper

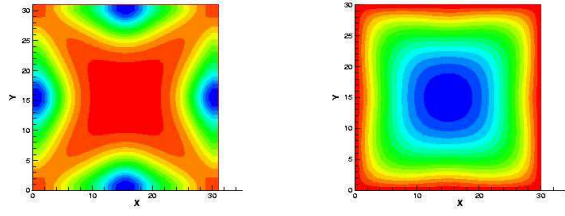
pairs, runs from 0 to 1, the level 1 corresponding to the full superconducting state. Each isolated group of contours is called a "vortex" representing the supercurrent \mathbf{J} circling around the vortex core, with $\Psi = 0$ at the vortex core. In the 3-D plots of Fig. 2 (b), it is clear that the vortices reach close to $|\Psi|^2 = 0$ at the core.

Note that the number of vortices increases in multiples of 4. This is a consequence of the fact that the vortices are symmetrically created at the mid-points of the sample edges. Perfect symmetry in the sample geometry dictates that each side creates an equal number of vortices. The symmetry manifests itself in this geometry-dominated problem, and vortices arrange themselves in the square-symmetric configurations. The resultant steady states are mostly not true equilibrium states since the vortex arrangements do not reflect the intrinsic tendency of vortices to form a triangular lattice known to appear in bulk samples. The natural next step is to add a thermal fluctuation term to find the true equilibrium states which may or may not conform with this symmetry. This approach would then be like simulated annealing.^{15,17} However, we believe it would not be practical to perfect this approach since it will likely be difficult to determine the appropriate rate of cooling and starting temperature. The run-time of the computer program might also be expected to be much longer than we have found here. So we have devised a different approach which we believe is much more efficient for finding the equilibrium states. This is given in a later section. We shall see that even the cases with low number of vortices are not the true equilibrium. Also of interest is the fact that for some H the vortex configuration has a much more difficult time to settle down, needing much longer run-times to get to a steady state. Geometry controls the settling time more than the energy in these cases.

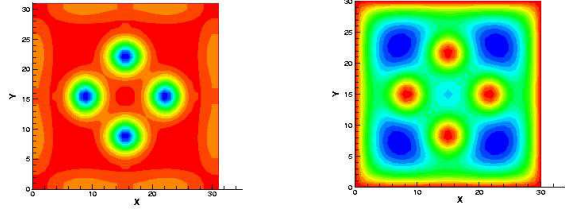
Our results are summarized in Table 1, which lists the range of H for each possible number of vortices and the induced magnetic field $B = \frac{1}{|\Omega|} \int_{\Omega} h d\Omega$. The H 's listed correspond to the threshold values for each range. They were found on a trial-and-error basis, and can be refined to any desired accuracy. Below $H = 0.839$, there is no vortex. Between $H = 0.84$ and 1.144 , the vortex number $n = 4$, and so on. Of course, these thresholds change as we change the sample size. For example, if we double the length of each side, $H = 1.0$ gives $n = 36$.

n	H	B
0	0.839	0.616350
4	0.84	0.733198
4	1.144	0.977913
8	1.145	1.069432
8	1.429	1.302241
12	1.43	1.379098
12	1.732	1.628862
16	1.733	1.698629
16	2.058	1.971973

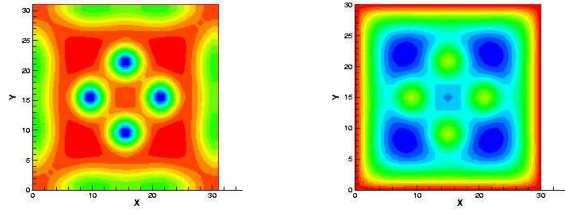
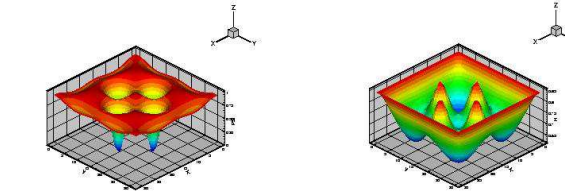
Table 1. The number of vortices n and the induced



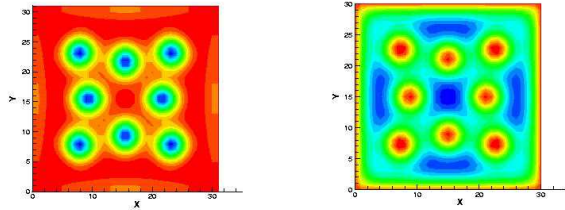
(a) $H = 0.839$



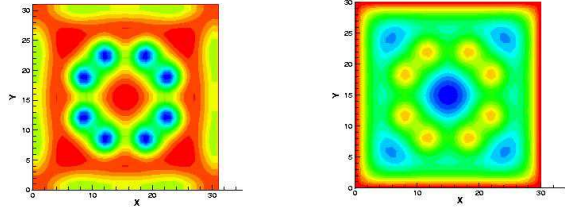
(b) $H = 0.840$



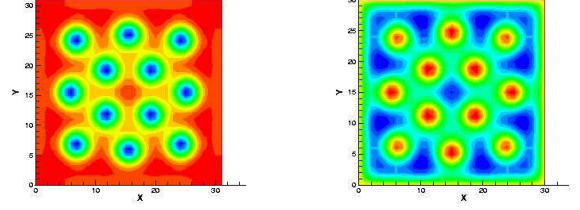
(c) $H = 1.144$



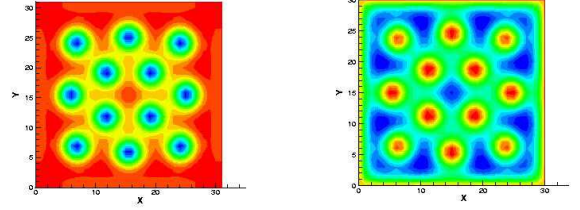
(d) $H = 1.145$



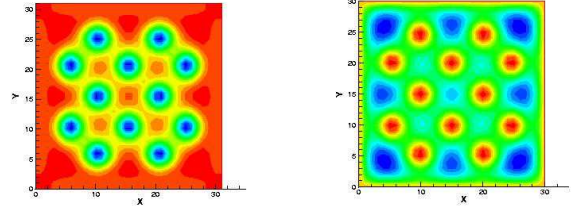
(e) $H = 1.429$



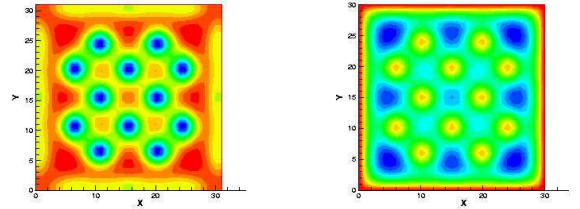
(f) $H = 1.430$



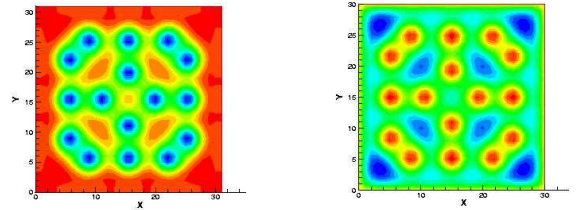
(g) $H = 1.454$



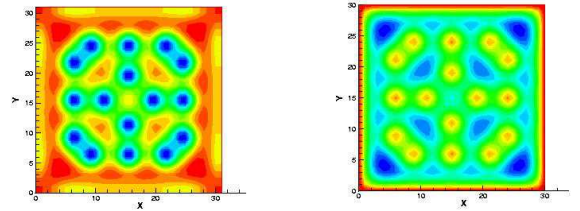
(h) $H = 1.455$



(i) $H = 1.732$



(j) $H = 1.733$



(k) $H = 2.058$

FIG. 2. Plots of $|\Psi|^2$ [left figures in (a) through (k)] and $h = \nabla \times \mathbf{A}$ [right figures in (a) through (k)] for various H .

magnetic field B for the applied magnetic field H .

The B vs H plot is shown in Fig. 3, and reveals an abrupt increase in B between the regions of different number of vortices. For example, when H changes from 1.144 to 1.145, B changes from 0.977913 to 1.069432. If the limit $\Delta H \rightarrow 0$ is taken, we expect a sudden configurational phase transition increasing the number of vortices, as is apparent in Figs. 2 (c) and (d). Such mini-first-order transitions are known to occur in a mesoscopic superconductor as H is changed,^{5–9} but the details are quite different, because different parameter (κ) regimes and sample geometries (cylinder vs. film) are studied.

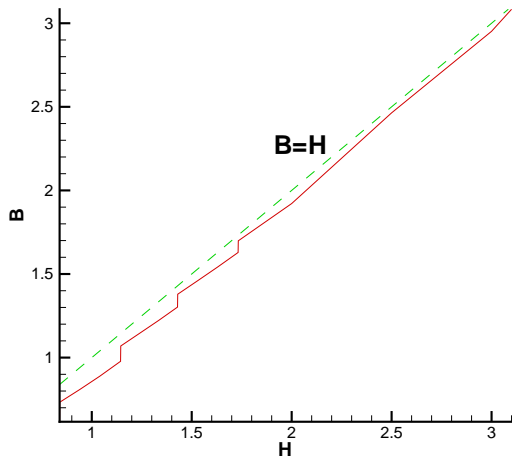


FIG. 3. plotted is B as a function of H .

Phase transition is also evident in the $n = 12$ case, where the vortex configuration shows a sudden change in arrangement even with the same number of vortices for a slight increase of the applied field from $H = 1.454$ to $H = 1.455$.

In the B vs H plot, B is much lower than H when the number of vortices is small, but as the vortices increase, the curve approaches the $B = H$ curve asymptotically. So for the given sample, the number of vortices and B increase as the applied magnetic field H increases. This reflects the fact that the vortices are a form of magnetic penetration.

V. TIME SEQUENCE SHOWING VORTEX ENTRY DYNAMICS

Fig. 4 shows plots of Cooper pair density for $H = 1.145$ in time. The number of vortices is 8. The perfect symmetry in the sample geometry dominates the transient process, but in the middle of the process the whole configuration makes a rotation to rearrange itself into a new configuration. (Note that time advances from 3000 to 17500 between the 8th and 9th frames.) The final result is still

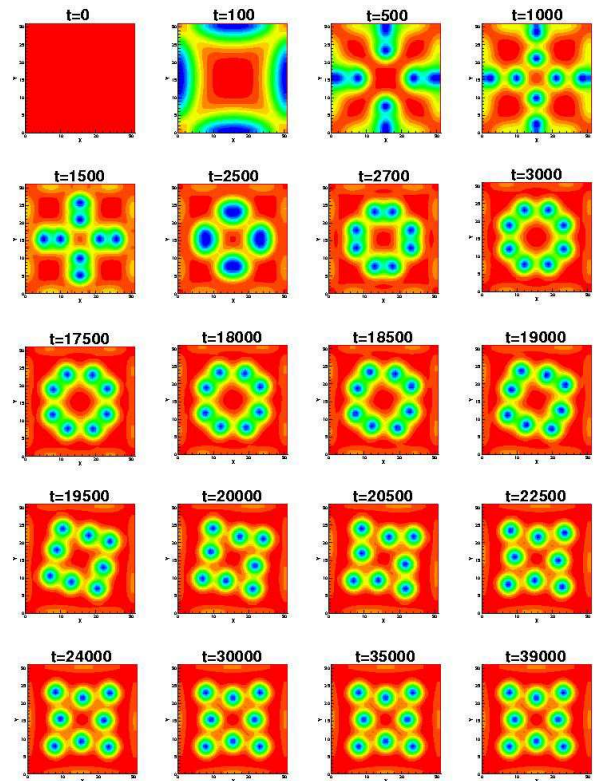


FIG. 4. Time sequence of vortex-entry dynamics for $H = 1.145$.

a square-symmetric configuration. We note that during the rotation process the vortex configuration loses some mirror symmetries of the sample but still preserves the 90° rotation symmetry. So these transient states do not possess the full symmetry of the sample. We think that this is possible because our numerical method has very weakly broken the sample symmetry. That is, we think that the state just before the rotation is a metastable state only within the subspace of configurations preserving the full symmetry of the sample. Thus, in the actual physical situation when the sample has perfect symmetry and the temperature is sufficiently low this rotation may take a very long time to take place. For samples with imperfect symmetry this relaxation time may be shorter. Since this is a symmetry-induced qualitative property of the vortex-entry dynamics in a mesoscopic superconductor, we believe its general validity is independent of the fact that we have obtained it by solving a simplified set of TDGL equations which are not truly physical.

VI. STEADY STATES WITH REDUCED SYMMETRY AND THE EQUILIBRIUM STATE

The previous sections present solutions for a mesoscopic type-II superconducting cylinder with initially no vortex inside the system. The validity of such solutions also requires a perfectly square sample without any de-

fect at the boundary, and temperature sufficiently low, so that thermal fluctuations are too weak to help the system find lower-energy configurations of reduced symmetry. This is an ideal condition, producing only solutions consistent with the sample symmetry, and, even during the transient, the system is bound to this symmetry (except in rare cases when the transient solutions can keep only fourfold rotation symmetry but not mirror symmetries — See Fig. 4). In principle, one can reproduce this ideal system in a laboratory with special care.

In real situations there most-likely exist some small defects or perturbations at the boundary. Then vortices can enter the system asymmetrically to produce steady-state configurations with reduced symmetry of lower total Gibbs energy than any symmetric solution. A strong enough thermal fluctuation could also change the vortex number and rearrange the vortices to such a configuration. In previous work, to take into account these perturbations, a random fluctuation term was added to the governing equation.²⁴ This term breaks the symmetry governing the equations, energizing the system to jump out of the local minima in energy, and over the energy barrier.³ But this increases the computing time greatly. (This method is basically what is called “simulated annealing”^{15,17} in computer science.)

As an alternative approach, we employ perturbed initial conditions instead of the perfectly superconducting initial condition, and is similar to Peeters et al.^{7,5} but with a new idea introduced to make the numerical scheme much more efficient:

We have first used randomly perturbed initial conditions. They can indeed lead to final steady-state solutions with reduced symmetry and lower energies. But we find this way is very inefficient for finding the equilibrium state at any given H . We have also tried to use a lower-symmetry configuration from such a calculation as the initial condition for a new H value, but find that the vortex number can often be trapped in an uncontrollable non-equilibrium value due to the existence of surface energy barriers against vortex entry or exit. So this method of adopting an existing solution as the initial condition can not be reliably used to find the true equilibrium state in a given system and field. (Peeters et al. changes the field in small steps to avoid this difficulty²⁵, but we believe the procedure to be unnecessarily tedious.)

To obtain the true equilibrium vortex configuration at any given magnetic field without employing some simulated annealing method, we have devised a systematic approach to generate initial states with given numbers of vortices at random distributions. It is through an analytic expression as follows: First, for one vortex at the origin in circular coordinates (r, θ) , we use the widely-known approximate expression^{26–28}

$$\Psi(r, \theta) = \frac{r e^{i\theta}}{\sqrt{r^2 + \kappa^{-2}}}. \quad (17)$$

Converting it to Cartesian coordinates, we can move the center of the vortex to any arbitrary position (x', y') by

simply replacing (x, y) by $(x - x', y - y')$. Denoting this expression as $\Psi_{x', y'}(x, y)$, an n -vortex expression can be simply constructed as

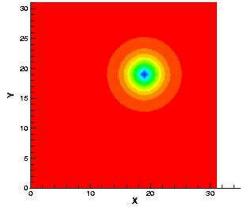
$$\Psi(x, y) = \Psi_{x_1, y_1}(x, y) \Psi_{x_2, y_2}(x, y) \cdots \Psi_{x_n, y_n}(x, y). \quad (18)$$

This expression obeys the important topological condition that the phase of Ψ must increase by 2π when any one vortex center is circumnavigated. The magnetic field inside the sample does not obey any topological condition, so it can be simply set equal to zero for the initial condition. The positions of the vortices can be generated using random number generators, only if they are inside the sample. This idea may seem to be simple, but it appears to have not been employed before. We illustrate below such initial conditions to obtain steady-state vortex configurations of any given numbers of vortices n . Comparing the total Gibbs energies of such solutions of different n , we can then determine the equilibrium vortex number and configuration. For illustrative purposes, we consider the case $H = 0.840$. In Fig. 5, the initial conditions for Ψ with 1 through 8 randomly-placed (artificial) vortices [the left figures in (a) through (o)], and the steady-state vortex configurations they evolve to [the right figures in (a) through (o)], are shown. The corresponding Gibbs free energies of these steady states are plotted in Fig. 6 as a function of the vortex number n . The minimum-energy configuration at $n = 5$ is seen to display the square-symmetry of a five-vortex configuration with a vortex in the center. Although we have not yet applied this scheme to other field values, the method we have devised to find the equilibrium vortex configurations for a given size and shape of the sample and different values of the external magnetic field should now be clear.

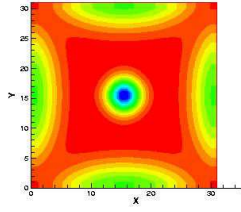
VII. SUMMARY AND CONCLUSION

A numerical scheme to study the mixed states in a mesoscopic type-II superconducting cylinder in a

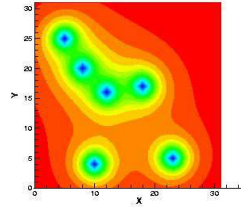
longitudinal external magnetic field H has been developed. It is based on solving a set of simplified time-dependent Ginzburg-Landau equations. We have first applied this scheme to the case of field penetration into a zero-field cooled sample. Case studies for various values of the external magnetic field are presented. Contour plots of the Cooper pair density, and the induced magnetic field inside the sample, display the magnetic vortex solution first discovered by Abrikosov, but in a small sample the vortex arrangement is not simply triangular. Giant vortices and anti-vortices are not found in this study, unlike previous studies of type-I mesoscopic thin films. (But at sufficiently high magnetic field we still expect the system to favor a single giant vortex at the center as it goes into a surface superconducting state, but only if the sample is not too small.) Since we start the solution with a uniformly superconducting initial condition,



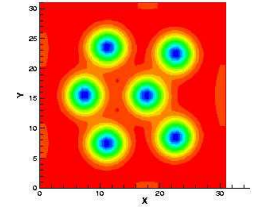
(a)



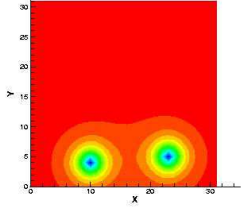
(b)



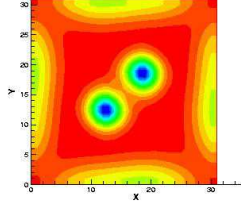
(c)



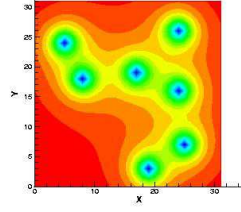
(g)



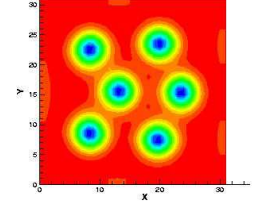
(d)



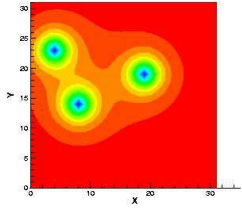
(e)



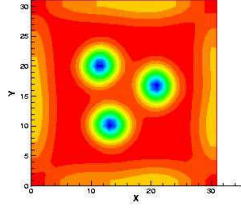
(h)



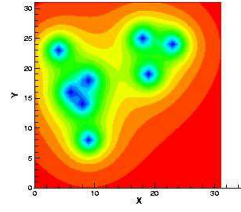
(i)



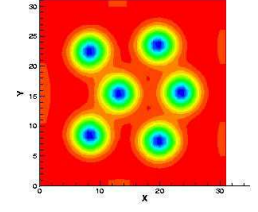
(f)



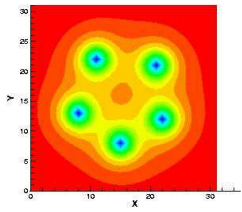
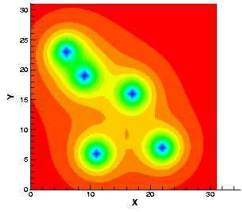
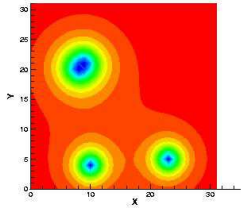
(j)



(k)



(l)



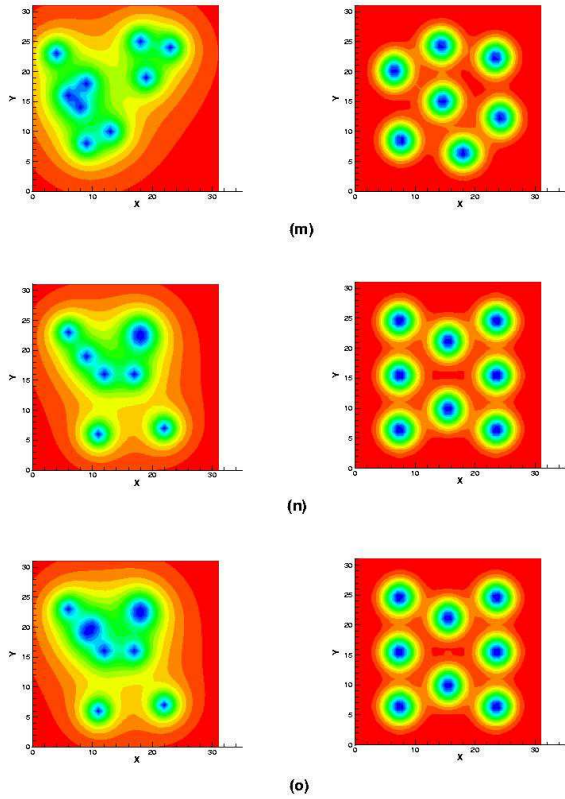


FIG. 5. The initial, random vortex configurations [left figure in (a) through (o)], and the corresponding steady-state vortex configurations they evolve to [right figure in (a) through (o)].

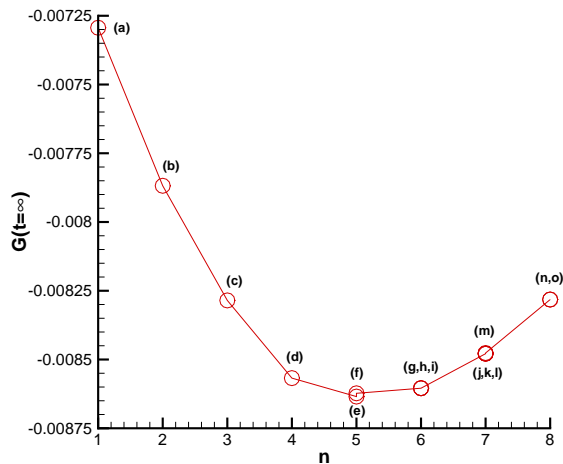


FIG. 6. The steady-state Gibbs free energy for various n .

and the sample has perfect square symmetry, both the number of vortices and their steady-state configurations are governed by the square sample geometry. Changes in the configuration and the number of vortices occur as H is varied through first-order configurational phase transitions, similar to those found earlier, but different in detail. This phase transition characteristic is confirmed by the contour plots, and jumps in the values of the induced magnetic field B at certain discrete H values. A time sequence shows that the system passes through intermediate configurations, and remains in some of them for a long time, eventually settling down to the steady-state configuration, which corresponds to the lowest-Gibbs-energy configuration consistent with the symmetry constraints to the vortex number and configuration. One could find the true equilibrium states, (which would appear in actual samples, when there are symmetry-breaking surface defects as vortex-nucleation centers, or when thermal fluctuation is sufficiently strong to move the system out of metastable states, but not too strong to melt the vortex lattice,) by adding additional terms in the equations to simulate thermal fluctuations, but here we have devised a different approach which we believe is more efficient. We introduce a way to generate analytic initial states of prescribed numbers of vortices, but allow their positions to be random. They evolve to steady-state vortex arrangements of all possible vortex numbers near the equilibrium number, from which we can compare total Gibbs energy to determine the equilibrium vortex number and configuration. In this way we can avoid the problem of surface and bulk energy barriers, which can trap the system in non-equilibrium vortex numbers and configurations — an undesirable situation which usually happens if one chooses the initial state randomly without controlling the vorticity quantum number L .

Acknowledgements Hu wishes to acknowledge the support from the Texas Center for Superconductivity and Advanced Materials at the University of Houston. Andrews acknowledges support from the Texas A&M University through the Telecommunications and Informatics Task Force.

¹ P. G. de Gennes, *Superconductivity in Metals and Alloys*, W. A. Benjamin, New York (1966). Reprinted by Addison-Wesley, Reading, MA (1989).

² S. J. Chapman, *SIAM Review* **42** 555 (2000).

³ M. Tinkham, *Introduction to Superconductivity* (McGraw-Hill, New York, 1996).

⁴ A. A. Abrikosov, *Zh. Eksp. Teor. Fiz.* **32** 1442 (1957) [*Sov. Phys. JETP* **5** 1174 (1957)].

⁵ B. J. Baelus and F. M. Peeters, *Phys. Rev. B* **65** 104515, (2002).

⁶ V. A. Schweigert and F. M. Peeters, *Phys. Rev. B* **57** 13817

- (1998).
- ⁷ V. A. Schweigert, F. M. Peeters, and P. Singha Deo, Phys. Rev. Lett. **81** 2783 (1998).
 - ⁸ P. Singha Deo, V. A. Schweigert, F. M. Peeters, and A. K. Geim, Phys. Rev. Lett. **79** 4653 (1997).
 - ⁹ J. Bonca and V. V. Kabanov, Phys. Rev. B **65** 012509 (2001).
 - ¹⁰ V. R. Misko, V. M. Fomin, J. T. Devreese, and V. V. Moshchalkov, Physica C **369**, 361 (2002).
 - ¹¹ K. Geim, S. V. Dubonos, J. J. Palacios, I. V. Grigorieva, M. Henini, and J. J. Schermer, Phys. Rev. Lett. **85**, 1528 (2000).
 - ¹² V. R. Misko, V. M. Fomin, J. T. Devreese, and V. V. Moshchalkov, Phys. Rev. Lett. **90**, 147003 (2003).
 - ¹³ In this brief survey of literature, we have not included solutions of linearized GL equations to study the vortex configurations near the phase boundary, studies of vortex configurations in the presence of pinning center(s), and studies based on the London approximation.
 - ¹⁴ G. W. Crabtree, D. G. Gunter, H. G., Kaper, A. E. Koshelev, G. K. Leaf, and V. M. Vinokur, Phys. Rev. **61**, 1446 (2000).
 - ¹⁵ W. H. Press, B. P. Flannery, S. A. Teukolsky, and W. T. Vetterling, *Numerical Recipes*, Cambridge University Press, Cambridge (1989). Sec. 10.9.
 - ¹⁶ As far as we know, previous approaches used random initial conditions with no control of L , so the magnetic field must be changed in very small steps to obtain speedy convergence. If so, the present scheme represents an important improvement, which allows direct implementation at any applied field. Note that the scheme also applies to the situation when a given distribution of pinning centers exist in the system or on its surface.
 - ¹⁷ M. M. Doria, J. E. Gubernatis, D. Rainer, Phys. Rev. B **41** 6335 (1990).
 - ¹⁸ For a larger sample in a sufficiently large magnetic field, we can occasionally obtain configurations with a reduced symmetry when solving the equations starting with the uniform superconducting state, but this is very rare, and very difficult to control. We think that this is because the numerical program does not observe the perfect square symmetry. But this violation of symmetry is a weak one. This way to get an asymmetric steady state is not reliable, so we do not recommend its use to find any asymmetric equilibrium state.
 - ¹⁹ Q. Du, M. D. Gunzburger, J. S. Peterson, SIAM Review **34** 54 (1992).
 - ²⁰ E. Coskun and M. K. Kwong, Nonlinearity **10** 579 (1997).
 - ²¹ S. L. Adler and T. Piran, Rev. Mod. Phys. **56** 1 (1984).
 - ²² H. G. Kaper and M. K. Kwong, J. Comp. Phys. **119** 120 (1995).
 - ²³ For a different way to discretize the problem without involving staggered grid, see Z. D. Wang and C. R. Hu, Phys. Rev. B **44** 11918 (1991).
 - ²⁴ R. Kato, Y. Enomoto, S. Maekawa, Phys. Rev. B **47** 8016 (1993).
 - ²⁵ F. M. Peeters, private communication.
 - ²⁶ A. Schmid, Phys. kondens. Materie **5** 302 (1966).
 - ²⁷ C.-R. Hu and R. S. Thompson, Phys. Rev. B **6** 110 (1972).
 - ²⁸ J. R. Clem, J. Low Temp. Phys. **18** 427 (1975).